ELSEVIER

Surface Science 449 (2000) 93–103

surface science

www.elsevier.nl/locate/susc

Co growth on Pt(997): from monatomic chains to monolayer completion

P. Gambardella [a,*], M. Blanc [a], L. Bürgi [a], K. Kuhnke [a], K. Kern [a,b]

[a] *Institut de Physique Expérimentale, Ecole Polytechnique Fédérale de Lausanne, CH-1015 Lausanne, Switzerland*
[b] *Max-Planck-Institut für Festkörperforschung, Heisenbergstr. 1, D-70569 Stuttgart, Germany*

Received 14 October 1999; accepted for publication 29 November 1999

Abstract

We have used the Pt(997) surface as a deposition template to grow high-density arrays (5×10^6 cm^{-1}) of parallel Co nanowires. We demonstrate that we can routinely grow ordered arrays of single monatomic chains of Co with precise coverage monitoring by in situ thermal energy atom scattering (TEAS). Nanowires constituted by one or more atomic chains have been characterized as a function of the substrate temperature and coverage by TEAS and scanning tunneling microscopy (STM). We find that, due to slow edge diffusion at low temperature and interlayer mass transport at high temperature, periodic arrays of uniform smooth chains are obtained only between 250 and 300 K. Co deposition in this temperature range results in a uniform coverage of chains having the same average width that can be used to investigate the magnetic properties of one-dimensional structures. The structure of a single-layer Co film has also been investigated: we show that the Co monolayer develops a non-periodic dislocation network upon deposition at 250 K. There is evidence for moderate Co incorporation into the first Pt layer below room temperature.

Keywords: Cobalt; Epitaxy; Growth kinetics; Nanowires; Platinum; STM; TEAS; Vicinal single crystal surfaces

1. Introduction

Atomic scale manipulation offers vast opportunities to investigate the interplay between magnetism, morphology, and chemical environment [1]. In particular, one-dimensional systems have recently been targeted as a test field involving open questions in the magnetism of such structures [2–5]. It is well known from theory that an isolated Ising-like monatomic chain cannot exist in a long-range magnetic ordered state at non-zero temperature [6]. However, little is known about more complex systems that are investigated in real experiments, typically supported arrays of quasi-one-dimensional stripes of bulk ferromagnetic materials on non-magnetic substrates. In these systems, hybridization with the supporting material, coupling between adjacent stripes and/or with the substrate do indeed give rise to different magnetic behaviors. Fe stripes formed by connected triangular-shaped islands on a stepped Cu(111) surface exhibit a pronounced temperature- and time-dependent magnetic behavior and out-of-plane anisotropy [2,3], while Fe stripes more than 20 atoms wide on vicinal W(110) show a relaxation-free magnetization with in-plane easy axis across the stripes [4,5]. None of these studies, however, has addressed the monatomic wire limit.

* Corresponding author. Fax: +41-21-693-3604.
E-mail address: pietro.gambardella@epfl.ch (P. Gambardella)

0039-6028/00/$ - see front matter
PII: S0039-6028(99)01218-2

In a recent paper, Dorantes-Dávila and Pastor [7] reported magnetic anisotropy energy calculations of free-standing and supported one-dimensional wires of 3d transition metals. Their results predict a strong magnetic anisotropy reduction in passing from free-standing wires to Pd(110)-supported wires, accompanied by a rotation of the easy axis of magnetization from the longitudinal to the transverse direction perpendicular to the substrate. While the chain length is not expected to have a strong influence on the magnetic anisotropy for Co chains longer than 20 atoms, different spatial arrangements of the Co chains can have a non-negligible effect. To address these and other structure-related questions that will be discussed later in this paragraph, we have chosen Co/Pt(997) as a model system to create arrays of supported nanowires. Since magnetic properties like anisotropy, spontaneous magnetization, and the temperature dependence of ordered magnetic states are highly structure-sensitive in low-dimensional systems [1,8], it is mandatory to characterize magnetic nanostructures down to the atomic scale.

This paper deals with the growth aspects of Co on vicinal Pt(111) surfaces. The combination of two complementary techniques such as thermal energy atom scattering (TEAS) and scanning tunneling microscopy (STM) offers the opportunity of investigating growth on a macroscopic scale with atomic-scale insight. We discuss the monatomic chain formation and diffusion-related phenomena, focusing on the conditions that allow the growth of equally spaced regular Co stripes. We describe the growth scenario up to monolayer completion and analyze the atomic structure of the Co monolayer film. Magnetic measurements on Co/Pt(997) will be the object of forthcoming publications. Spin-resolved photoemission measurements on Co/Pt(997) show that the Co atoms maintain their individual magnetic moments while in contact with the Pt step edges. The monatomic chains display a magnetic exchange splitting but no remanence down to 100 K [9].

Pt(997) is a stepped surface of remarkable uniformity that can be used as a template for the self-assembly of nanowires [10,11]. Monatomic steps separate terraces that have an average width $w = 20.1$ Å with standard deviation $\sigma = 2.9$ Å. An STM image of the Pt(997) surface is shown in Fig. 1. Upon step decoration, the short step separation results in arrays of parallel wires that have a density of 5×10^6 cm^{-1}. Regular patterns of parallel wires and such high densities are key issues for the employment of integral techniques to probe the magnetism of monatomic wires. The coverage corresponding to a single monatomic chain decorating each step of the Pt(997) surface is 0.13 ML, which is within the detection sensitivity of state-of-the-art surface magnetism probes.

Although a lot of interest has been dedicated to thin Co/Pt layered structures due to the pronounced perpendicular magnetic anisotropy that makes this system a good candidate for high-density magneto-optical devices [12–16], relatively few studies [17–19] reported an atomic-scale analysis of the Co—Pt interface. Details of the interface atomic structure, such as strained layers, stacking faults, steps and intermixing can give sizable contributions to the magnetic anisotropy, favoring or inhibiting its perpendicular component [1,12,14, 16,18,20–23]; given that the separation of such contributions is still controversial, it would be useful to measure anisotropy-related quantities on well-defined Co/Pt interfaces whose differences are

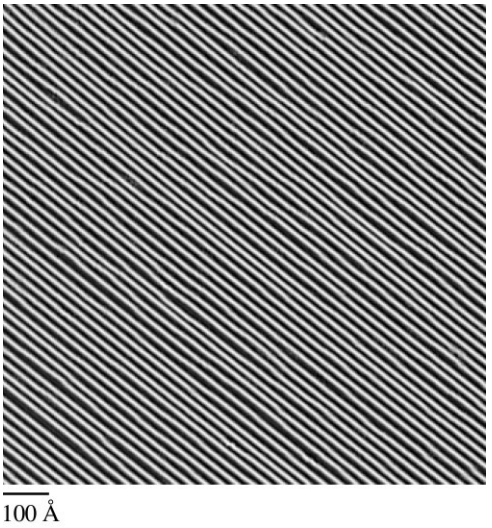

Fig. 1. $\partial z/\partial x$ image of the clean Pt(997) surface. Tunneling current $I = 1.0$ nA, sample bias $V = 0.6$ V. The average terrace width is 20.1 ± 2.9 Å. The step edges are represented by white lines; the step down direction is from the upper right corner to the lower left one.

well known, such as Co on flat and vicinal Pt(111) surfaces. In order to characterize the Co/Pt interface on a stepped substrate we have investigated the monolayer structure by STM and TEAS. As expected from the strong lattice mismatch and from the negative intermixing enthalpy between Pt and Co, the monolayer film reveals a partially dislocated structure with a small degree of alloying even below room temperature (RT). The work presented in this paper constitutes to our knowledge the first study of Co nucleation on a densely stepped Pt surface and it is the first publication to consider Co deposition on Pt below RT.

As shown in a previous STM study [17], Co on Pt(111) nucleates in a spatially homogeneous way at RT and grows in a quasi-layer-by-layer mode up to 3 ML. After 3 ML, three-dimensional growth with hcp stacking sets in. A number of depressions are observed in the first Co layer that are attributed to non-specified misfit dislocations. For $T \geq 300$ K Co induces a reconstruction of the Pt(111) surface in the form of Pt fcc and hcp domains. The reconstruction has been attributed to Co atoms incorporated in the first Pt layer by a strain-relief process. Post-deposition nucleation of dendritic islands removes the Pt reconstruction. A recent STM study suggests that the dendrites mainly consist of Pt atoms that have been replaced in the underneath layer by Co atoms [19]. Surface X-ray diffraction measurements [18] confirm that Co grows quasi-layer-by-layer in the first layers, but, contrary to Ref. [17], suggest that Co grows with its own lattice spacing already from the first layer at RT. On Pt(997), on the other hand, our measurements clearly show that Co grows in a strained fashion preserving the underlying Pt lattice spacing up to $T \approx 350$ K. We found clear evidence for two different kinds of dislocation in the form of hcp–fcc stacking faults, and for what we attribute to Co inclusions in the Pt layer. The growth of monatomic and multi-atomic Co chains is reported in Sections 3.1 and 3.2, respectively; the Co—Pt interface corresponding to 1 ML Co coverage is discussed in Section 3.3.

2. Experiment

The thermal energy He atom scattering experiments have been carried out in a triple-axis spectrometer [24,25] that allows an independent variation of the incidence and reflection angle between 30 and 90°. The He beam spot on the sample is of the order of 5 mm^2, thereby probing a macroscopic portion of the sample. The Pt(997) surface is prepared in situ in the scattering chamber by repeated cycles of 800 eV Ar^+ sputtering and annealing to 850 K, followed by a brief exposure to 1×10^{-7} mbar oxygen and by a flash to $T > 1000$ K to remove eventual carbon contaminant. The sample must be cooled at a slow rate (<40 K/min) down to 500 K in order to avoid step-bunching and step-meandering. The surface cleanliness is checked by Auger and He reflectivity measurements; the base pressure in the scattering chamber is 1×10^{-10} mbar. Cobalt is evaporated on the surface by e-beam heating of a Co rod; the pressure in the chamber never rises to more than 3×10^{-10} mbar during deposition.

The STM images have been recorded in a different experimental setup, a home-built STM [26] which consists of a variable temperature preparation–evaporation stage and a low-temperature microscope operated at 77 K during this work. Sputtering and evaporation procedures were identical to the ones employed in the He scattering experiments. The base pressure in the preparation and STM chambers was below 1×10^{-10} mbar. The coverages between the He and STM setups have been cross-calibrated by the Co Auger peak intensities relative to Pt using two identical Auger spectrometers.

TEAS on vicinal surfaces produces a diffraction pattern whose maxima are located at the Bragg positions corresponding to the reciprocal superlattice of the step array. Once the scattering parameters have been fixed, i.e. the incidence angle θ_i, the reflection angle θ_f (see Fig. 2), and the He beam wavelength λ_{He}, the in-plane variations of the diffraction peak intensities depend only on the surface topmost layer structure [27,28]. Oscillations of the intensity of one such peak during deposition are related to the number of diffuse scatterers on the surface [27,29]. As we discussed in a recent paper, the sensitivity to different surface sites varies depending on the scattering geometry [10,30]. On vicinal surfaces,

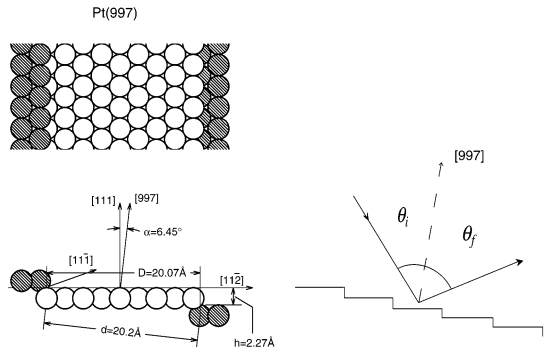

Fig. 2. Scheme of the Pt(997) terrace atomic structure and of the He beam scattering geometry.

grazing incidence conditions (large θ_i values) greatly enhance step sensitivity, while scattering angles closer to the surface normal probe the surface ordering as a whole. Fig. 3 shows two deposition curves for Co on Pt(997) at $\theta_i = 52.8^\circ$, $\theta_f = 40.1^\circ$ (top) and $\theta_i = \theta_f = 83.0^\circ$ (bottom). The upper curve has two maxima which we attribute to the completion of the first and second Co monolayer, respectively. We use the first maximum to calibrate the coverage scale. This calibration yields a coverage of 0.13 ML for the first peak in the grazing incidence curve (bottom) that has been measured with the same deposition rate at 300 K. Since 0.13 ML corresponds to the coverage of a single monatomic row decorating each step of the Pt(997) surface, we attribute this peak to the completion of the first Co monatomic chain. By monitoring Co deposition with TEAS in grazing incidence conditions we thus have a means to detect in real-time the formation of monatomic chains at the step edges. However, peaks corresponding to the formation of subsequent Co rows cannot be detected by TEAS, even if the STM measurements show that row-by-row growth continues at least up to 0.6 ML. As discussed elsewhere [11], when mass transport between different terraces is inhibited, wider terraces complete a given number of rows earlier than narrower ones; an apparently small standard deviation of ~ 3 Å in the terrace width distribution is sufficient to smear out the reflectivity peaks for the second and further rows.

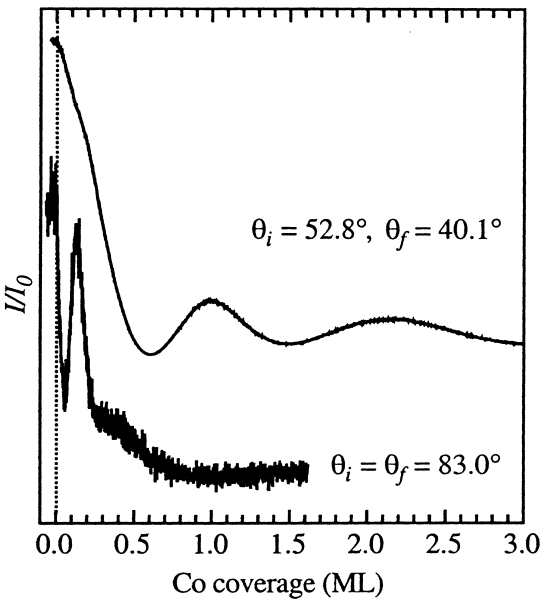

Fig. 3. Normalized TEAS intensity during deposition of Co at $\theta_i = 52.8^\circ$, $\theta_f = 40.1^\circ$ (top) and $\theta_i = \theta_f = 83.0^\circ$ (bottom). The He beam wavelength λ_{He} is 1.03 Å. Terrace contribution to the He intensity diminishes with increasing scattering angle. The oscillations in the upper curve correspond to the completion of two subsequent Co monolayers and serve as coverage calibration. The peak in the grazing incidence curve (bottom) corresponds to the formation of the first Co atomic row along the Pt steps. The deposition rate is 1.6×10^{-3} ML s^{-1} for both curves. The upper curve is recorded at $T = 250$ K while the lower one is recorded at $T = 300$ K.

3. Results and discussion

3.1. Growth of Co monatomic chains

To determine the influence of growth kinetics on Co row formation, a series of TEAS deposition curves was recorded at grazing incidence for different temperatures (Fig. 4). We note that no influence of the deposition rate on the growth mode was observed for rates between 3×10^{-4} ML s^{-1} and 6×10^{-3} ML s^{-1} at $T = 250$ K. By following the temperature evolution of the intensity maximum around 0.13–0.20 ML in Fig. 4, we observe that the first Co row decorates the Pt steps between 150 and 500 K. However, the formation of a true one-dimensional atomic chain cannot be inferred by the sole presence of this intensity maximum. Else we would expect to

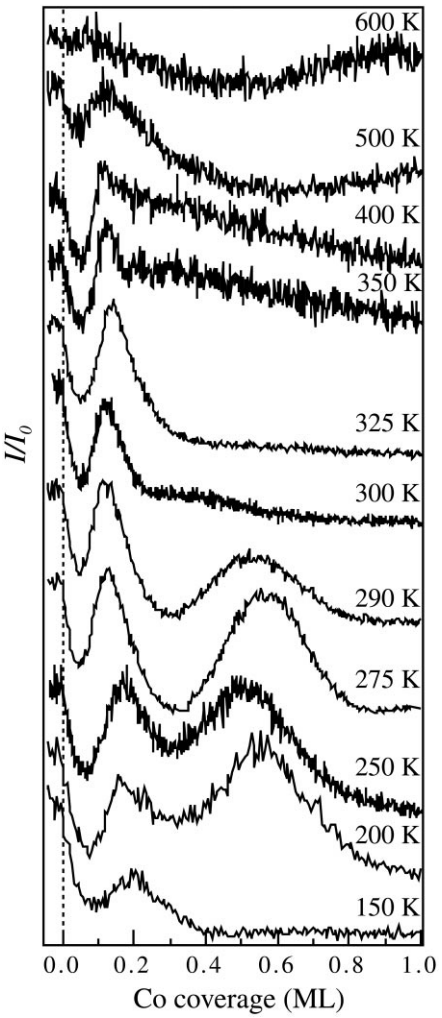

Fig. 4. TEAS intensity in grazing incidence conditions during Co deposition at different temperatures; $\theta_i = \theta_f = 83°$, $\lambda_{He} = 1.01$ Å. The first peak around 0.13–0.20 ML corresponds to the monatomic decoration of the Pt steps by Co atoms. The coverage scale has been calibrated with the procedure described in Section 2. The deposition rate is between 1.6×10^{-3} and 4.2×10^{-3} ML s^{-1} for all curves.

observe a maximum always at 0.13 ML, the nominal coverage corresponding to the pseudomorphic decoration of the Pt steps by single monatomic chains on Pt(997). At 150 K the first row peak is quite broad and centered at 0.2 ML. As in the case of Ag and Cu at 120 K [11] we conclude that the growth mode is rough because of kinetically inhibited edge-smoothening. Rough growth implies that the adatoms attaching to Co already decorating the Pt step edges are not mobile enough to migrate to the remaining bare Pt sites. The diffusion barriers relevant for edge-smoothening are not only due to Co—Co edge diffusion, but most likely due to the crossing of Co corner atoms involving a loss in coordination for the migrating adatom. To find the threshold at which smooth row growth occurs, we have plotted in Fig. 5 the coverage corresponding to the first intensity maximum in Fig. 4 vs. substrate temperature; one can see that only for $T > 250$ K does the first peak correspond to the monatomic row nominal coverage of 0.13 ML, which is expected for fast diffusion of the Co adatoms. Data are also reported for Ag and Cu chains as in Ref. [11] to show that this is a general phenomenon. The STM image in Fig. 6, taken after deposition of 0.07 ML Co at 250 K, shows atomically-resolved Co monatomic chains decorating the Pt step edges. Co rows grow on the lower step edge side, as in most cases of step decoration in metal systems [4,11,31–33], but contrary to Fe on Cu(111) [3]. A few protrusions can also be seen on the Pt terraces in Fig. 6; we suggest that these protrusions, that are ~ 0.3 Å higher than the surrounding Pt atoms, represent small

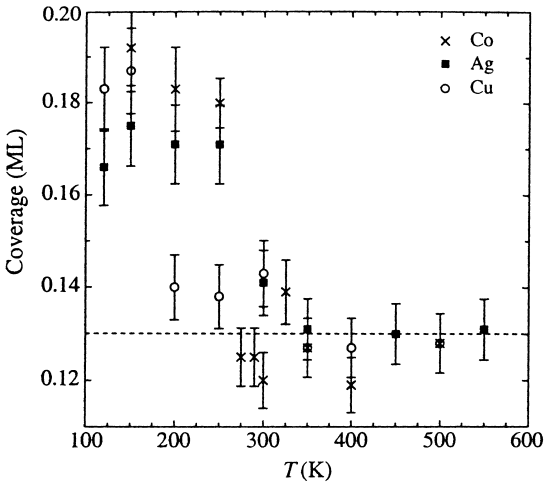

Fig. 5. Coverage corresponding to the first peak in Fig. 4 vs. deposition temperature. Slow edge diffusion shifts the first row peak towards higher coverages. The nominal coverage of a single monatomic wire is 0.13 ML as indicated by the dashed line. The Ag and Cu data shown here for comparison are taken from Ref. [11].

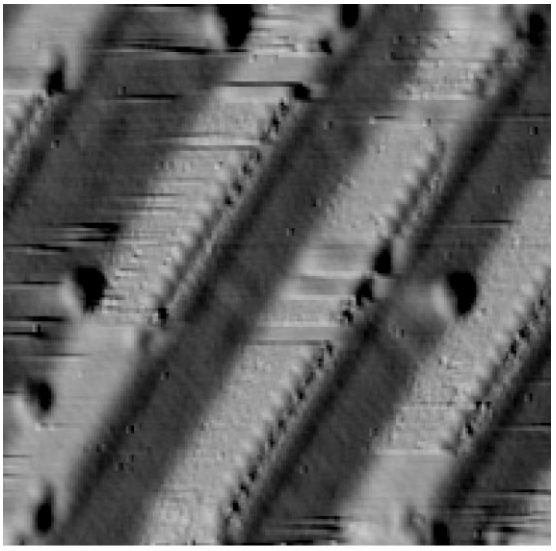

Fig. 6. $\partial z/\partial x$ image taken after deposition of 0.07 ML Co at 250 K. Atomically-resolved Co chains decorate the step edges. Step down direction is from right to left. The protrusions on the terraces might be due to Co atoms incorporated in the Pt layer. $I=1.0$ nA, $V=0.1$ V.

inclusions of Co in the Pt layer. At present, however, we cannot definitively assign these features to Co atoms embedded in the Pt layer as our Auger sensitivity to contaminants is $\sim 1\%$ of a monolayer, close to the observed coverage of such features. Further support for moderate intermixing between Co and Pt at low temperature will be given in Section 3.3.

In the high temperature range, step decoration is limited by the onset of alloying between Co and Pt. X-ray diffraction and LEED studies [18,34,35] of Co films on Pt(111) have shown that alloying sets in at 550 K. In agreement with these measurements we do not observe step decoration at 600 K (see Fig. 4) and the ratio between the Co and Pt Auger peak intensities decreases accordingly.

3.2. Growth of Co stripes

We now describe Co growth beyond the monatomic chain limit. Particular attention is paid to those growth conditions that allow us to prepare samples with uniformly spaced arrays of regular Co stripes. The fabrication of stripes with regular smooth edges is important in order to address the transition from 1D to 2D behavior in, e.g., magnetism studies without dealing with geometrically complex growth patterns. Although raising the substrate temperature might be effective in smoothening the Co stripes, one has to take care that the Co atoms remain confined to their adsorption terraces. Only in this case, in fact, will the periodic arrangement of the substrate be preserved and the average width of the Co stripes can be taken to be $w\Theta_{\mathrm{Co}} \pm \sigma\Theta_{\mathrm{Co}}$ where w is the average terrace width, σ the standard deviation of the terrace width distribution, and Θ_{Co} is the Co coverage.

We start from the analysis of Fig. 4 for $\Theta_{\mathrm{Co}} \geq 0.13$ ML. As discussed in Section 2, the desynchronization of the row growth on terraces having different widths suppresses reflection maxima due to chain formation apart from the first one. However, between 200 and 290 K we observe a second peak centered at ~ 0.5–0.6 ML. The intensity of this half-monolayer peak is the result of a narrowed step distance distribution at $\Theta_{\mathrm{Co}} \approx 0.5$ ML [11]. If the Co atoms are confined to their nucleation terraces (forbidden interlayer mass transport), the terrace width distribution narrows with increasing Co coverage and reaches a minimum at $\Theta_{\mathrm{Co}} = 0.5$ ML. This happens because in this regime short terraces grow at the expense of larger adjacent ones, a so-called debunching effect [36]. The presence of the half-monolayer peak is therefore a signal of good surface periodicity, as confirmed by the comparison of the STM images in Figs. 7a and 8.

For $T < 200$ K edge diffusion is too slow to allow rearrangement of the Co adatoms in regular stripes and no half-monolayer peak is observed in Fig. 4. Deposition in this temperature range is likely to produce connected Co islands with irregular triangular shapes attached to the Pt steps, as has been observed by STM for the Ag/Pt(997) system at $T = 120$ K [11]. In agreement with our results, Boragno et al., in a yet unpublished STM study of Co nucleation on Pt(111) [37], have found that Co islands grow randomly ramified at $T = 130$ K and that the mobility-driven transition to compact-shaped clusters starts between 160 and 200 K. As the substrate temperature increases,

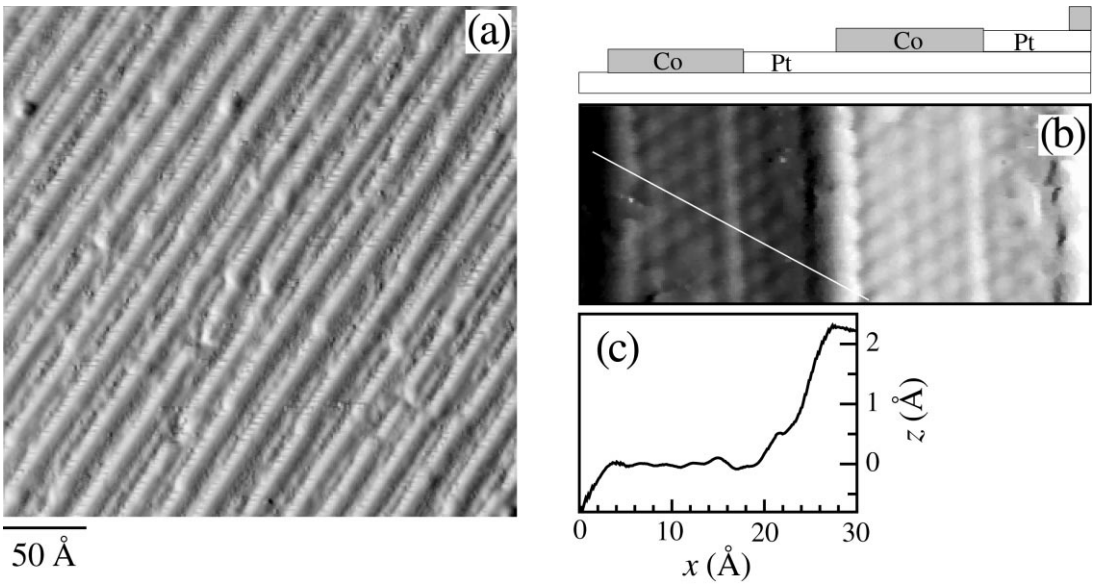

Fig. 7. (a) STM $\partial z/\partial x$ image of 0.6 ML Co deposited at $T=250$ K; step down direction is from right to left; $I=1.0$ nA, $V=0.1$ V. (b) Detail of two adjacent terraces, $I=4.0$ nA, $V=1$ mV; the drawing shows the corresponding vertical cross-section. (c) Line scan showing the small height difference between Co and Pt. Depending on the tunneling parameters and tip conditions Co can be imaged a few tenths of an angstrom higher or lower than Pt [17,19,37]; in the present work the Co layer is found to be in most cases 0.2–0.4 Å higher than Pt as in (b). Due to the finite tip size, atoms on the lower step edge side are often distorted or not imaged at all; this effect is evident in the line scan reported in (c), where the rising edge extends itself over more than one lattice spacing.

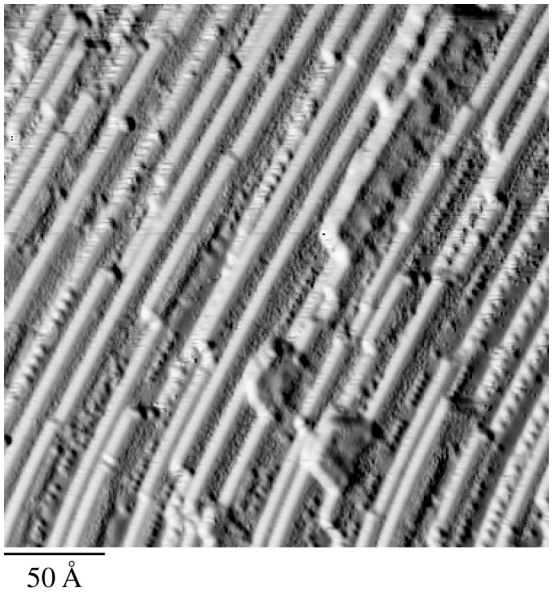

Fig. 8. $\partial z/\partial x$ image of 0.6 ML Co deposited at $T=385$ K. In contrast to Fig. 7a the periodic step pattern is partly lost because interlayer mass-transport allows the formation of double-layer Co stripes. $I=1.0$ nA, $V=0.1$ V.

smoothening occurs and assists the formation of regular parallel stripes. Fig. 7a is an STM image recorded after deposition of 0.6 ML Co showing that Co growth at $T=250$ K conserves the original step pattern, forming regular stripes that run parallel to the Pt steps. The half-monolayer peak in Fig. 4 suddenly disappears between 290 and 300 K. Such a net transition has a counterpart in the Co growth mode. Co adatoms at $T\geq 300$ K have enough thermal energy to cross the Pt—Co boundary at steps, thereby disrupting the high step periodicity that was at the origin of the half-monolayer peak. Fig. 8 shows such an effect following 0.6 ML Co deposition at 385 K. Irregular step bunching is also observed, indicating that Co tends to form bilayer islands. The temperature at which Co atoms can cross over the Co—Pt lateral interface at steps gives us an estimate for the diffusion barrier of such a process. By assuming the threshold temperature at which the barrier is completely overcome as the temperature where crossing takes place once per second, we can calculate the diffusion barrier E_h for this process

to be

$$E_h = \ln(v_0) k_B T \quad (1)$$

where k_B is the Boltzmann constant and v_0 is the usual prefactor. By taking $v_0 = 10^{13}$ and $T = 300$ K we estimate E_h to be of the order of 0.7 eV.

In contrast to the deposition of Co on Pt(111) [17,19,37], we do not observe the formation of dendrite-like islands above 300 K; reconstruction and exchange processes between Co and Pt are nonetheless not excluded and will be discussed in Section 3.3. The fabrication of periodic arrays of Co regular stripes is limited at low temperature by slow diffusion processes and at high temperature by the migration of Co atoms across adjacent terraces, a process which is active already at 300 K.

3.3. 1 ML Co

When a complete Co layer is formed, dislocations develop on part of the surface; this is evident already at 250 K. The dislocation pattern consists of fcc–hcp stacking faults that run parallel to the step edges (Fig. 9a) and of triangular shaped structures whose arms intersect the steps at an angle of $\pm 60^\circ$ (Fig. 9b). Since the dislocations do not form an ordered superstructure they do not give rise to additional diffraction peaks in the He spectrum, contributing only in lowering the reflectivity of the Co monolayer.

The arrow in Fig. 9 evidences the transition between fcc and hcp domains along the dislocation (a). The formation of stacking faults is attributed to a strain-relief mechanism arising from the 9.7% lattice mismatch between Co and Pt. However, in terms of strain relief one would expect the domain boundaries to be perpendicular to the steps because strain is supposedly higher along the atomic rows running parallel to the step edges than along the short perpendicular ones. The formation of domain boundaries parallel to the step edges can be attributed to the presence of a lateral interface between Pt and Co. Since Pt—Co heterobonds are stronger than Co—Co bonds at the step edges [38], the first Co row is probably shifted towards the Pt step with respect to an ideal pseudomorphic overlayer; as a result of this shift the amount of strain in the direction perpendicular to the substrate steps can be increased in a considerable way and give rise to dislocations.

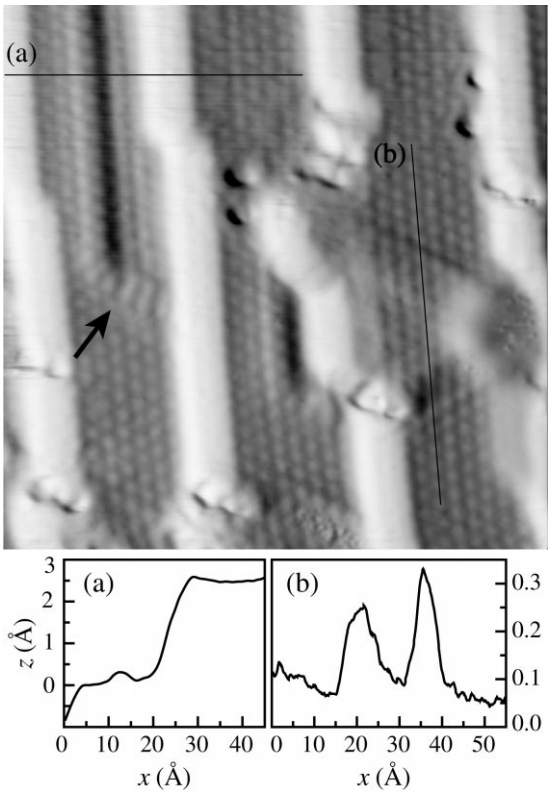

Fig. 9. $\partial z/\partial x$ image of 1 ML Co deposited at $T = 250$ K; $I = 1.0$ nA, $V = 8$ mV. Two different dislocated domains are clearly visible. (a) An hcp–fcc stacking fault runs parallel to the step on the left; the arrow evidences the transition between fcc and hcp stacking. (b) A triangular shaped structure whose arms intersect the step edges at $\pm 60^\circ$.

The analysis of the triangular structures (b) is not conclusive. Recent tight-binding calculations [39] indicate that the optimal structure of a Co monolayer on Pt(111) is constituted by a superlattice of alternating fcc–hcp equilateral triangular regions, separated by local line defects extending over two contiguous atomic rows. This suggests that the observed triangular dislocation in Fig. 9 is a domain boundary between fcc and hcp regions. On the other hand, the stacking transition between the exterior and the interior of the triangle is not as evident as for (a). Alternatively, since Co atoms appear higher in the STM images than Pt atoms (see Fig. 7), the positive height difference between

the triangle sides and the rest of the terrace could be attributed to Co atoms on top of Co incorporated in the Pt underlying layer.

Co incorporation upon deposition at 300 K was reported by Lundgren et al. [19] and low-temperature intermixing has been reported for similar systems such as Pt/Ni [40,41].

Supporting evidence (see also Fig. 6) for exchange processes between Pt and Co below room temperature is given in Fig. 10: a Co island on the lowest terrace on the left has nucleated on top of 1 ML Co at 250 K. Its height difference with respect to the Co atoms on the adjacent terrace (which preserve the Pt interlayer spacing) is 0.3 Å, the same as measured for the protrusions found on the terraces. This suggests that the protrusions in Fig. 10 are actually Co atoms on top of incorporated Co, as sketched at the bottom.

We now discuss the Co—Co spacing in the monolayer film. He scattering on a vicinal surface, in addition to the diffraction peaks due to the step periodic structure, gives rise to Bragg peaks due to the atomic corrugation of each terrace. Knowing

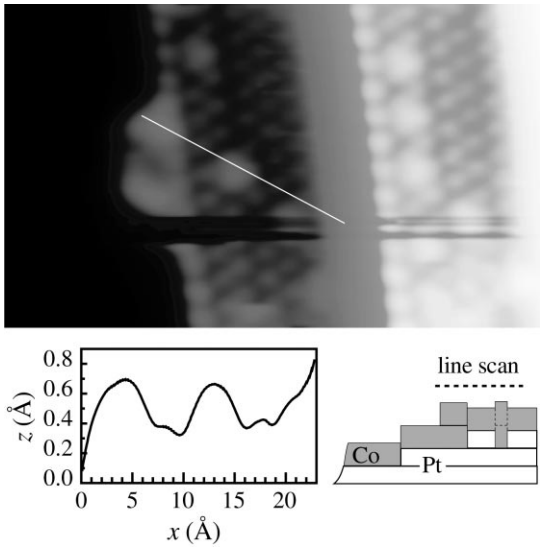

Fig. 10. Image of 1 ML Co taken at $T=250$ K; $I=6.0$ nA, $V=4$ mV. A Co island nucleating on top of the first Co layer is visible attached to the middle step. The height of the Co island is the same as that of the protrusions on the terrace, suggesting that the latter result from Co atoms incorporated in the Pt substrate, as depicted in the drawing. The horizontal lines in the lower half of the STM image are due to a tip instability.

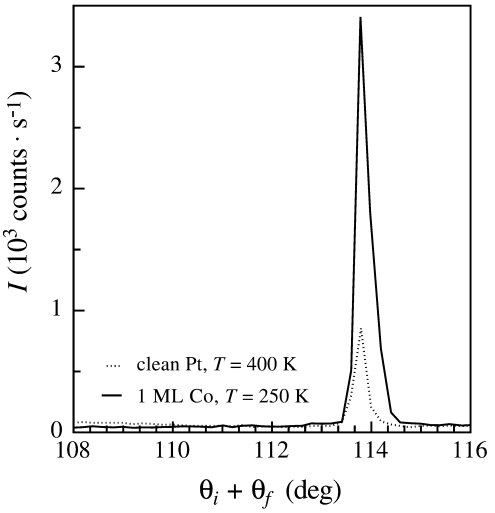

Fig. 11. First-order Bragg peak relative to the terrace atomic structure measured for clean Pt at 400 K (dotted line) and 1 ML Co at 250 K (solid line). The incidence angle is kept fixed while the reflection angle is varied. The Bragg incidence and reflection angles corresponding to the peak are 34.8 and 79.0°, respectively, measured with respect to the (111) direction; $\lambda_{He}=0.98$ Å.

the He beam wavelength, the angular position of one of these peaks allows us to determine the lateral lattice constant of the topmost layer of the surface. In Fig. 11 the dotted line is the first-order Bragg peak of a clean Pt surface at 400 K. From its position we calculate a spacing between neighboring atomic rows running along the $[1\bar{1}0]$ direction (parallel to the steps) of 2.39 ± 0.05 Å, which is very close to the theoretical value of 2.40 Å. The solid line is a spectrum recorded after deposition of 1 ML Co at 250 K; since the angular position is the same, we conclude that most of the first Co layer at this temperature has the same lattice spacing as the Pt substrate, in agreement with the calculation for the Co/Pt(111) system reported in Ref. [39].

4. Conclusions

We have investigated deposition on Pt(997) as a means to obtain densely packed arrays of parallel Co monatomic wires. TEAS measurements allow real-time monitoring of the wire coverage with

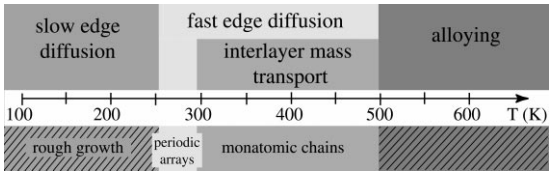

Fig. 12. Diagram representing different Co growth modes on Pt(997) as a function of the substrate temperature. Although the temperature scale refers to the Co/Pt(997) system, this description applies to other metals such as Ag and Cu on Pt(997) [11].

submonatomic row precision. Co row-by-row growth has been characterized with respect to the substrate temperature during deposition. We found that the decoration of the Pt steps by Co atoms takes place in a wide range of temperatures: from 150 to 500 K, when alloying sets in. However, for $T \leq 250$ K slow edge-diffusion limits the smoothening of the Co chains. At 300 K Co atoms have enough thermal energy to cross the Co—Pt lateral interface at the steps, thereby allowing the formation of double layer Co stripes and the breaking of the original periodic step patterns. The temperature window for the growth of a regular periodic pattern of Co wires is therefore limited to a narrow interval between 250 and 300 K when edge diffusion is fast enough to have perfect row-by-row growth and interlayer crossing is still inhibited. These results are summarized in Fig. 12. There is some evidence for Co incorporation into the Pt top layer already at 250 K. At monolayer completion strain causes the formation of stacking faults at 250 K; most of the Co layer is, however, in registry with the Pt substrate at this temperature. Heating above 350 K results in relaxation of the Co spacing due to the formation of bilayer Co islands.

Acknowledgements

P.G. would like to thank H. Brune and C. Carbone for stimulating discussions and O. Jeandupeux for his help with the STM setup. P.G. also acknowledges financial support from the University of Genova, Italy.

References

[1] F.J. Himpsel, J.E. Ortega, G.J. Mankey, R.F. Willis, Adv. Phys. 47 (1998) 511 and references cited therein.
[2] J. Shen, R. Skomski, M. Klaua, H. Jenniches, S. Sundar Manoharan, J. Kirschner, Phys. Rev. B 56 (1997) 2340.
[3] J. Shen, M. Klaua, P. Ohresser, H. Jenniches, J. Barthel, C.V. Mohan, J. Kirschner, Phys. Rev. B 56 (1997) 11 134.
[4] H.J. Elmers, J. Hauschild, H. Höche, U. Gradmann, H. Bethge, D. Heuer, U. Köhler, Phys. Rev. Lett. 73 (1994) 898.
[5] J. Hauschild, H.J. Elmers, U. Gradmann, Phys. Rev. B 57 (1998) R677.
[6] N.D. Mermin, H. Wagner, Phys. Rev. Lett. 17 (1966) 1133.
[7] J. Dorantes-Dávila, G.M. Pastor, Phys. Rev. Lett. 81 (1998) 208.
[8] U. Gradmann, in: K.H.J. Buschow (Ed.), Handbook of Magnetic Materials Vol. 7/1, Elsevier, Amsterdam, 1993, pp. 1–96.
[9] A. Dallmeyer, C. Carbone, W. Eberhardt, C. Pampuch, O. Rader, W. Gudat, P. Gambardella, K. Kern, Phys. Rev. B 61 (2000) 5133.
[10] V.E. Marsico, M. Blanc, K. Kuhnke, K. Kern, Phys. Rev. Lett. 78 (1997) 94.
[11] P. Gambardella, M. Blanc, H. Brune, K. Kuhnke, K. Kern, Phys. Rev. B 61 (2000) 2254.
[12] P.F. Carcia, J. Appl. Phys. 63 (1988) 5066.
[13] W.B. Zeper, F.J.A.M. Greidanus, P.F. Carcia, C.R. Fincher, J. Appl. Phys. 65 (1989) 4971.
[14] C.H. Lee, R.F.C. Farrow, C.J. Lin, E.E. Marinero, C.J. Chien, Phys. Rev. B 42 (1990) 11 384.
[15] N.W.E. McGee, M.T. Johnson, J.J. de Vries, J. aan de Stegge, J. Appl. Phys. 73 (1993) 3418.
[16] T. Kingetsu, J. Appl. Phys. 76 (1994) 4267.
[17] P. Grütter, U.T. Dürig, Phys. Rev. B 49 (1994) 2021.
[18] S. Ferrer, J. Alvarez, F. Lundgren, X. Torrelles, P. Fajardo, F. Boscherini, Phys. Rev. B 56 (1997) 9848.
[19] E. Lundgren, B. Stanka, W. Koprolin, M. Schmid, P. Varga, Surf. Sci. 423 (1999) 357.
[20] C. Chappert, P. Bruno, J. Appl. Phys. 64 (1988) 5736.
[21] C.H. Lee, H. He, F.J. Lamelas, W. Wavra, C. Uher, R. Clark, Phys. Rev. B 42 (1990) 1066.
[22] B.N. Engel, M.H. Wiedmann, R.A. Van Leeuwen, C.M. Falco, Phys. Rev. B 48 (1993) 9894.
[23] D. Weller, G.R. Harp, R.F.C. Farrow, A. Cebollada, J. Sticht, Phys. Rev. Lett. 72 (1994) 2097.
[24] K. Kuhnke, E. Hahn, R. David, P. Zeppenfeld, K. Kern, Surf. Sci. 272 (1992) 118.
[25] H. Schief, PhD Thesis, Ecole Polytechnique Fédérale de Lausanne, 1995.
[26] O. Jeandupeux, L. Bürgi, A. Hirstein, H. Brune, K. Kern, Phys. Rev. B 59 (1999) 15 926.
[27] B. Poelsema, G. Comsa, Helium Atom Scattering From Surfaces, Springer Tracts in Modern Physics Vol. 115 Springer, Berlin, 1989.

[28] E. Hulpke (Ed.), Helium Atom Scattering from Surfaces, Springer Series in Surface Science, Vol. 27, Springer, Berlin, 1991.
[29] B. Poelsema, A.F. Becker, G. Rosenfeld, R. Kunkel, N. Nagel, L.K. Verheij, G. Comsa, Surf. Sci. 272 (1992) 269.
[30] M. Blanc, K. Kuhnke, V. Marsico, K. Kern, Surf. Sci. 414 (1998) L964.
[31] M. Mundschau, E. Bauer, W. Swiech, J. Appl. Phys. 65 (1989) 581.
[32] T. Jung, Y.W. Mo, F.J. Himpsel, Phys. Rev. Lett. 74 (1994) 1641.
[33] J. de la Figuera, M.A. Huerta-Garnica, J.E. Prieto, C. Ocal, R. Miranda, Appl. Phys. Lett. 66 (1995) 1006.
[34] M.C. Saint-Leger, R. Baudoing-Savois, M. De Santis, P. Dolle, Y. Gauthier, Surf. Sci. 418 (1998) 485.
[35] A. Atrei, U. Bardi, M. Galeotti, G. Rovida, M. Torrini, E. Zanazzi, Surf. Sci. 339 (1995) 323.
[36] D. Kandel, J.D. Weeks, Phys. Rev. Lett. 74 (1995) 3632.
[37] C. Boragno, H. Röder, H. Brune, K. Kern, unpublished results.
[38] P. Gambardella, M. Blanc, K. Kuhnke, K. Kern, F. Picaud, C. Ramseyer, C. Girardet, C. Barretau, D. Spanjaard, M.C. Desjonqueres, unpublished results.
[39] C. Goyhenex, G. Tréglia, Surf. Sci. 446 (2000) 272.
[40] G.L. Kellogg, Phys. Rev. Lett. 67 (1991) 216.
[41] G.L. Kellogg, Phys. Rev. Lett. 76 (1996) 98.